Interference of the complex between NCS-1 and Ric8a with phenothiazines regulates synaptic function and is an approach for fragile X syndrome

Alicia Mansilla[a,1], Antonio Chaves-Sanjuan[b,1], Nuria E. Campillo[c], Ourania Semelidou[d], Loreto Martínez-González[c], Lourdes Infantes[b], Juana María González-Rubio[b], Carmen Gil[c], Santiago Conde[e], Efthimios M. C. Skoulakis[d], Alberto Ferrús[a], Ana Martínez[c], and María José Sánchez-Barrena[b,2]

[a]Departamento de Neurobiología del Desarrollo, Instituto Cajal, Spanish National Research Council, 28002 Madrid, Spain; [b]Departamento de Cristalografía y Biología Estructural, Instituto de Química Física Rocasolano, Spanish National Research Council, 28006 Madrid, Spain; [c]Centro de Investigaciones Biológicas, Spanish National Research Council, 28040 Madrid, Spain; [d]Division of Neuroscience, Biomedical Sciences Research Centre Alexander Fleming, 16672 Vari, Greece; and [e]Instituto de Química Médica, Spanish National Research Council, 28006 Madrid, Spain

Edited by Gregory A. Petsko, Weill Cornell Medical College, New York, NY, and approved December 23, 2016 (received for review July 7, 2016)

The protein complex formed by the Ca^{2+} sensor neuronal calcium sensor 1 (NCS-1) and the guanine exchange factor protein Ric8a coregulates synapse number and probability of neurotransmitter release, emerging as a potential therapeutic target for diseases affecting synapses, such as fragile X syndrome (FXS), the most common heritable autism disorder. Using crystallographic data and the virtual screening of a chemical library, we identified a set of heterocyclic small molecules as potential inhibitors of the NCS-1/Ric8a interaction. The aminophenothiazine FD44 interferes with NCS-1/Ric8a binding, and it restores normal synapse number and associative learning in a *Drosophila* FXS model. The synaptic effects elicited by FD44 feeding are consistent with the genetic manipulation of NCS-1. The crystal structure of NCS-1 bound to FD44 and the structure–function studies performed with structurally close analogs explain the FD44 specificity and the mechanism of inhibition, in which the small molecule stabilizes a mobile C-terminal helix inside a hydrophobic crevice of NCS-1 to impede Ric8a interaction. Our study shows the drugability of the NCS-1/Ric8a interface and uncovers a suitable region in NCS-1 for development of additional drugs of potential use on FXS and related synaptic disorders.

fragile X syndrome | synapse regulation | NCS-1 | protein–protein interaction inhibitor | X-ray crystallography

The fragile X syndrome (FXS) is the most common inherited neurological disorder causing intellectual disability and autism. FXS affects ∼1 in 2,500–5,000 men and 1 in 4,000–6,000 women and remains without effective pharmacological treatment (1–4). Thus, the discovery of new targets and drugs that could normalize mental abilities is a great current challenge. The causative mutation of almost all known cases of FXS is a trinucleotide cytosine–guanine–guanine (CGG) expansion in the 5′ UTR of the fragile X mental retardation gene (*fmr1*), resulting in loss of the fragile X mental retardation protein (FMRP). FMRP is an RNA binding protein that regulates the transport and translation of mRNAs. FMRP interacts directly with about one-third of the mRNAs that encode the synaptic proteome (5). However, this scenario of pleiotropy has been challenged recently by suggesting that the primary target of FMRP is the Diacylglycerol kinase kappa (Dgkκ), which would trigger a subsequent cascade of synaptic effects, in particular, on the glutamatergic type (6). Although the issue would require additional analysis, independent of whether the effects are direct or indirect, the FMRP transcriptome has identified mRNA targets associated with autism spectrum disorders (ASDs), mood disorders, and schizophrenia, which suggest potential common pathways for these clinically different diseases.

A recurrent feature in all of these diseases is a deviation in the synaptic equilibrium that defines normalcy. Either excess or deficit in the number of synapses can lead to pathology. In the case of FXS, cortical neurons of patients or *fmr1* KO mice show postsynaptic spines at increased density and with long-neck morphology, which have been interpreted as defects in synapse maturation or pruning (7–10). Similar spine effects are reported for ASDs (11). Benefiting from the conservation of the *fmr1* gene, work in *Drosophila* has shown that loss of function mutations increase synapse number, whereas the excess of function condition yields the opposite effect, synapse loss (12, 13). As for human subjects, *fmr1* mutants in *Drosophila* are deficient in associative learning and memory (14, 15).

During the past two decades, intense efforts have been made to understand the molecular and cellular events underlying synaptic dysfunction in FXS. Studies in animal models have revealed defects in multiple neurotransmitter systems and related signaling pathways (1–4). These studies have led to the development of potential therapeutic agents that target (*i*) neurotransmitter/neuromodulator systems (such as metabotropic glutamate receptors, mGluRs, or GABAergic receptors), (*ii*) signaling pathways downstream of neurotransmitter receptors (such as MAPKs, PI3K, mTOR, and GSK3), (*iii*) proteins regulated by FMRP (such as

Significance

Neurons coregulate their number of synapses and the probability of neurotransmitter release per synapse in an antagonistic manner. The binding of neuronal calcium sensor 1 (NCS-1) to the guanine exchange factor protein Ric8a coregulates these neuronal features. This study identified a small molecule, the phenothiazine FD44, that binds the interaction surface between NCS-1 and Ric8a, preventing the formation of the complex. Tested on a *Drosophila* model of the fragile X syndrome, where the number of synapses is in excess, FD44 proves effective to reduce synapse number to normal levels and restore normal learning performance. Our structure–function study shows the specificity of this compound and the drugability of the NCS-1/Ric8a interface for the treatment of fragile X and possibly, other synaptopathies.

Author contributions: A. Mansilla, N.E.C., O.S., C.G., E.M.C.S., A.F., A. Martínez, and M.J.S.-B. designed research; A. Mansilla, A.C.-S., N.E.C., O.S., L.M.-G., L.I., J.M.G.-R., C.G., E.M.C.S., A. Martínez, and M.J.S.-B. performed research; S.C. contributed new reagents/analytic tools; A.F., A. Martínez, and M.J.S.-B. analyzed data; and A.F. and M.J.S.-B. wrote the paper.

Conflict of interest statement: The Spanish National Research Council has filed a patent application (P201531358) with the Spanish Patent Office on the use of FD44 and derivatives as regulators of synaptopathies. A. Mansilla, N.E.C., C.G., A.F., A. Martínez, and M.J.S.-B. are listed as inventors.

This article is a PNAS Direct Submission.

Data deposition: The atomic coordinates and structure factors have been deposited in the Protein Data Bank, www.wwpdb.org [PDB ID codes 5AAN (FD44), 5FYX (FD16), and 5G08 (CPZ)].

[1]A. Mansilla and A.C.-S. contributed equally to this work.

[2]To whom correspondence should be addressed. Email: xmjose@iqfr.csic.es.

This article contains supporting information online at www.pnas.org/lookup/suppl/doi:10.1073/pnas.1611089114/-/DCSupplemental.

MMP9 or PAK), and (*iv*) the endocannabinoid system (1–4). It is likely that additional therapeutic targets will be designed, if feasible, against Dgkκ (6). Targeting FMRP or perhaps, even Dgkκ may not be a convenient strategy, because FMRP is also involved in the differentiation of neurons in the adult olfactory bulb and the hippocampus (16). Likewise, targeting the excess of postsynaptic mGlu receptors may also lead to secondary effects from the unbound excess of toxic glutamate and the imbalance between synapse number and amount of neurotransmitter released.

Under the current knowledge, it seems advisable to design potential therapies targeting the down-regulation of synapse number rather than the reduction of the number of neurons or neurotransmitter receptors (17). However, normal neuronal function requires tight control of probability of neurotransmitter release per synapse in addition to control of synapse number. Indeed, both neuronal properties are coregulated in an antagonistic manner (18, 19). Neurons with a high number of release sites usually manifest a low probability of release per site and vice versa. Thus, a potentially effective approach should target the signaling mechanism of this coregulation. Recently, we described the mechanism by which the Ca^{2+} sensor neuronal calcium sensor 1 (NCS-1; originally named Frequenin in *Drosophila*) interacts with the guanine exchange factor protein Ric8a to activate Gα proteins and coregulate synapse number and activity (18, 19). Interestingly, vertebrate NCS-1 mRNA has been identified as one of the FMRP targets (5), and Frequenin mRNA expression is decreased in the *Drosophila fmr1* mutant (20).

The available structural information on NCS-1/Ric8a recognition (19) and the function of the complex in synapse number control and probability of release led us to search for small compounds that could dock into the NCS-1/Ric8a interface to inhibit complex formation. We hypothesized that such compounds will decrease synapse number in FXS animal models and eventually, patients. Targeting protein–protein interactions (PPIs) has emerged as a viable approach in modern drug discovery. However, the identification of small molecules that effectively interrupt PPIs presents significant challenges (21). Here, we present biochemical, structural, and functional data showing that the aminophenothiazine derivative FD44 binds NCS-1 and inhibits its interaction with Ric8a. Furthermore, this compound mediates recovery of normal synapse number and improves associative learning in a *Drosophila* fragile X model. The crystal structure of NCS-1 bound to FD44 and the structure–function relationship study developed with close analogs explain the mechanism of action and the biological activity of this compound. This study shows the druggability of the NCS-1/Ric8a interface and the potential use of the aminophenothiazine FD44 as a drug candidate to treat FXS and related synaptic disorders.

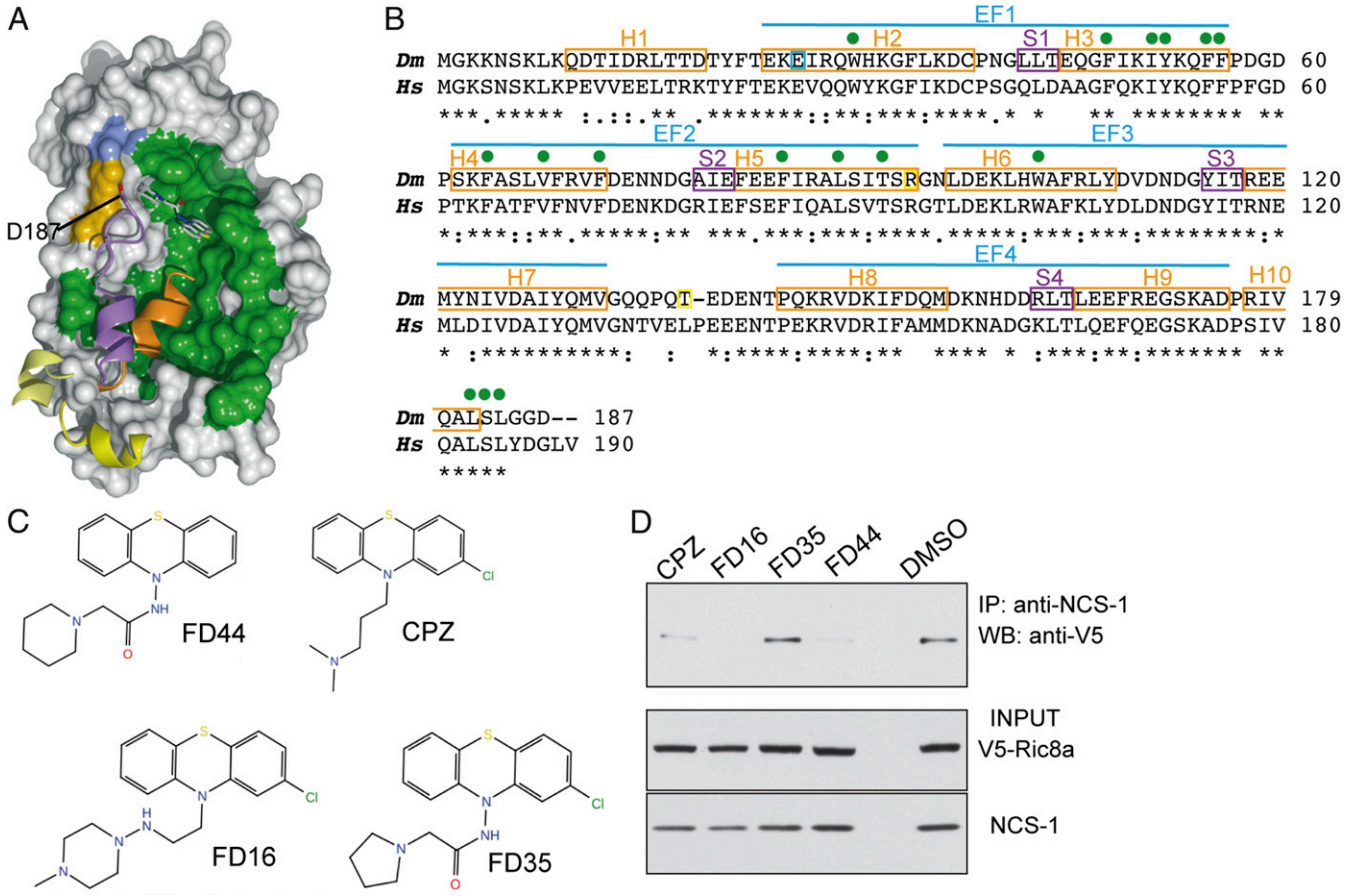

Fig. 1. VS calculations and validation of the inhibitory properties of the small molecule hits. (*A*) Predicted complex between human NCS-1 and FD44 by VS. FD44 molecule is displayed as sticks. Diagram shows the molecular surface of human NCS-1 [PDB ID code 1G8I, molecule A (23)], with the hydrophobic crevice in green; residues R94 and E26 in orange and blue, respectively; and helix H10 in lilac ribbon with D187 in sticks. The *Drosophila* ligand-free NCS-1 structures [4BY4 and 4BY5 (19)] have been superimposed, and helix H10, with its three different orientations inside or outside the crevice (orange and yellow ribbons, respectively), is shown to indicate its mobility. (*B*) Sequence alignment of human and *Drosophila* NCS-1 proteins. Secondary structure elements and EF-hand location of the crystallographic dNCS-1/FD44 structure are indicated. The amino acids implicated in FD44 recognition are shown as green circles. R94 and T138 are highlighted with yellow rectangles, and E26 is with a blue rectangle. EF, EF hand; H, helices; S, strands. (*C*) Structure of the aminophenothiazine molecules with high score in the VS. (*D*) Co-IP binding assay of human NCS-1 and V5-tagged Ric8a in transfected HEK cells in the presence of the small compounds and the vehicle DMSO. IP, immunoprecipitation; WB, Western blot.

Results

Virtual Screening for Small Molecules. We reported previously that *Drosophila* NCS-1 (dNCS-1; also known as Frq2) and Ric8a interact to regulate synapse number and neurotransmitter release and that this interaction is reproduced by the human homologs (19). Although the structure of the NCS-1/Ric8a complex is unknown, our structural data on Frq2 followed by a mutagenesis study shed light on the molecular mechanism of Ric8a recognition by NCS-1 (19). We found that R94, located at the N-terminal edge of a hydrophobic crevice, is essential for the interaction with Ric8a (Fig. 1*A*). In addition, T138 proved important for Ric8a recognition. T138 is located in a mobile loop between helices H7 and H8 (Fig. 1*B*), 40 Å opposite to R94, at the C-terminal edge of the crevice (19). Thus, the NCS-1/Ric8a interaction requires this crevice, in particular the two amino acids located at each end. Furthermore, we showed the key role that helix H10 plays in this protein–protein binding, functioning as a built-in competitive inhibitor. Deletion of this mobile helix, which is found inserted into the crevice or solvent-exposed in the ligand-free dNCS-1 structure (Fig. 1*A*), increases the affinity for Ric8a (19). R94 is located in helix H5 (Fig. 1*B*; see Fig. 3), and its guanidinium group interacts with E26, located in helix H2, thus attaching helix H2 to the rest of the structure and contributing to the shape of the upper sidewall of the hydrophobic crevice. Because R94 is essential for Ric8a binding and reasoning that it might provide the key for developing targeted PPI inhibitors (22), we focused the search for small molecule candidates able to interrupt the NCS-1/Ric8a interaction at the R94 region.

The virtual screening (VS) through our in-house chemical library, composed of over 1,000 small heterocyclic compounds, was centered at the R94 environment of human [Protein Data Bank (PDB) ID code 1G8I (23)] and *Drosophila* [PDB ID code 4BY4, molecule B (19)] NCS-1 structures. Because of the motility of helix H10, which has been found inside the crevice (19, 24, 25), solvent-exposed (19), or parallel to the crevice (23) (Fig. 1*A*), it was not considered in the VS. It is interesting to note that the orientation of helix H10 in human NCS-1 (hNCS-1), caused by the crystallization conditions and the entrance of PEG molecules inside the crevice, permits the interaction of D187 with R94 (Fig. 1*A*) (23). This interaction occludes R94, an essential amino acid for Ric8a recognition, which should be solvent-exposed to interact with its target (19). In this case, deletion of helix H10 was necessary to allow better recognition of the small molecules by the R94 region. Results from VS were similar with either the human or the *Drosophila* structures and showed aminophenothiazine derivatives as candidate hits (Fig. 1 *A* and *C* and Table S1). We selected for additional studies only those molecules that showed a good score value together with a plausible distance to R94 (Table S1): FD35, FD16, FD44, and chlorpromazine (CPZ). These compounds, sharing the same tricyclic phenothiazine central scaffold, were previously known for their butirylcholinesterase inhibition in vitro and neuroprotective activity in cell assays (26, 27). The main structural differences among them are in the substituent attached to the heterocyclic nitrogen atom and in the presence or not of chlorine atoms in some of the benzene moieties. Although FD35, FD16, and FD44 are only research tools that may or may not become a human drug, the discovery of the Food and Drug Administration-approved drug CPZ in our VS encouraged us to go further with this study.

Binding and Toxicity Assays of Candidate Small Molecules. To assay the interaction between human Ric8a and NCS-1 in the presence of the selected candidates, we carried out binding assays in HEK cell cultures (*Materials and Methods* and Fig. 1*D*). Cells were cotransfected with human NCS-1– and Ric8a-expressing constructs. Each compound was tested separately at a final concentration of 20 μM. The data show that FD16, FD44, and CPZ inhibit the NCS-1/Ric8a interaction, whereas FD35 does not seem to affect complex formation. During preparation of the corresponding solutions, it was evident that the compounds could be ranked CPZ, FD44, FD16, and FD35 in decreasing order of solubility. The lack of efficacy observed after treatment with FD35 may result from its low solubility.

To quantify the binding interference of FD44 and FD16, we carried out dose–response assays (Fig. 2 *A* and *B*). Throughout the range of drug concentrations applied to the transfected HEK cells, it became evident that FD44 is a more effective inhibitor of NCS-1/Ric8a binding than FD16. In addition, toxicity assays in HEK cell cultures showed that FD44 and FD16 are much better tolerated than CPZ (Fig. 2*C*), a feature required for an eventual use in therapy.

CPZ and related commercialized drugs are well-known in pharmacy because of their effects as antipsychotic agents. They show a strong affinity for dopamine D1 and D2 and adrenergic α_1 and α_2 receptors, and they function as their antagonists (28). To determine if FD44 is different from CPZ, radio-ligand displacement assays were performed with the receptors (Table S2) (www.cerep.fr/Cerep/Users/index.asp). These experiments provide an in vitro measurement of the interactions that occur between a receptor and a small molecule, FD44 in this case, by analyzing the ability of the molecule to inhibit the binding of the receptors to specific control compounds. At 10 μM, FD44 does not inhibit the binding of control antagonists (Table S2), indicating that FD44 activity is completely different to that shown by its structural analog CPZ (28).

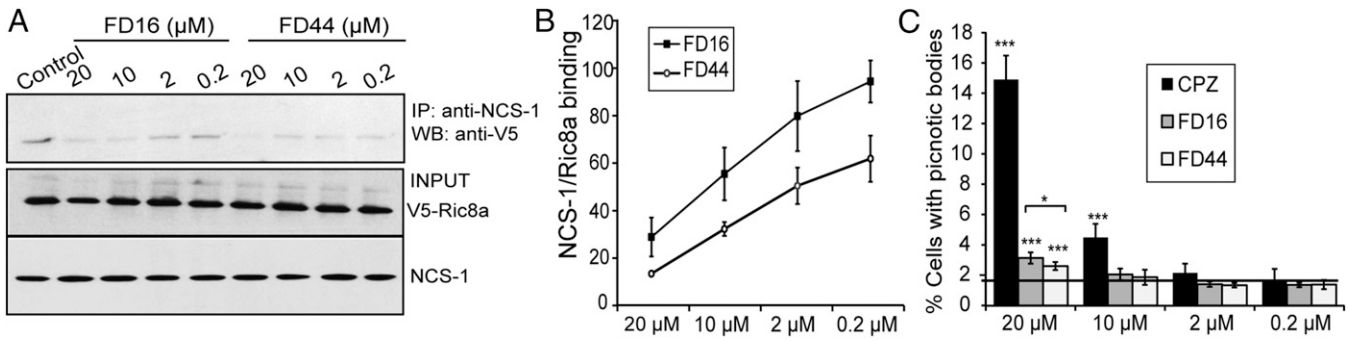

Fig. 2. Comparative binding and toxicity assays for FD44 and related molecules. (*A*) Binding assay of HEK cells cotransfected with human NCS-1 and V5-tagged Ric8a. IP, immunoprecipitation; WB, Western blot. (*B*) Graph representing the densitometry of bands from the co-IP of three independent assays. The binding interference dosage–response assay over a range of drug concentrations shows that FD44 is a more effective inhibitor compared with FD16. Data ± SEM. (*C*) Quantification of cell toxicity as HEK cells with picnotic bodies treated with FD44, FD16, or CPZ over the same range of concentrations. FD44 is the least toxic. The horizontal line marks the basal apoptosis in untreated HEK cell cultures. Data ± SD from three independent experiments.

The Structure of NCS-1 Bound to Ca^{2+} and the Aminophenothiazine FD44 or Close Analogs. To better understand the binding blockade properties of the candidate molecules, we crystallized the complex of dNCS-1 bound to FD44, FD16, and CPZ and solved their corresponding structures at 1.60-, 1.80-, and 1.52-Å resolution, respectively, using molecular replacement methods (Table S3). Crystals belonged to space group $P2_12_12_1$, and one complex was found in the asymmetric unit. Despite that Ca^{2+} was not added to the crystallization solution and that the protein sample was extensively dialyzed against Milli-Q water, the quality of the electron density maps clearly showed that the three functional EF hands (EF2, EF3, and EF4) contained Ca^{2+}. The well-defined pentagonal–bipyramidal coordination (29) together with the anomalous signal observed at the three EF hands unambiguously showed the presence of Ca^{2+} and discarded the presence of Mg^{2+} (Fig. S1*A*). The overall structure of dNCS-1 is nearly identical in FD44, FD16, and CPZ complexes, with differences confined to the binding site. The rmsd of FD44 and FD16 structures is 0.6 Å, whereas that of FD44 and CPZ is 0.9 Å.

Interestingly, the electron density map of the dNCS-1/FD44 complex clearly indicated that the small compound was located at the N-terminal region of the hydrophobic groove as VS calculations predicted but in a different orientation (Figs. 1*A* and 3 *A* and *B*) because of the presence of helix H10 that was avoided in the VS. The phenothiazine moiety in FD44 has a butterfly conformation, and the central six-membered ring has a boat conformation (Fig. S1*B*). The angle between planes of the two benzene rings is 118°. The structure around the nitrogen atom is almost planar, where the sum of the angles on the nitrogen atom is 358°. FD44 is deeply inserted in a pocket, and the contact area is 341.5 $Å^2$ (30). The conformation of this small heterocyclic molecule permits a large number of interactions with the protein, mainly van der Waals contacts with hydrophobic residues placed in helices H2, H3, H4, H5, H6, and H10 (Figs. 1*B* and 3*C*). The cavity where the aminophenothiazine is located can be described as a hydrophobic cage, where F48, V68, F72, and W103 constitute the base; Y52, F56, and F64 constitute the right-hand sidewall; F85, L89, and T92 constitute the left-hand sidewall; L182 and L184 constitute the lower sidewall; and I51 constitutes the upper sidewall. W30, F55, and S183 close the pocket from above, functioning as a lid (Fig. 3 *C* and *D*). Interestingly, the lid residue W30 stabilizes its side-chain conformation through a water-mediated H bond with R94 (Fig. 3*C*), the key amino acid for Ric8a recognition (19). Furthermore, T92, Y52, F55, and L182 play an important role in recognition of FD44. (*i*) T92 contacts the FD44 carbonyl group through a strong water-mediated H bond and a weak H bond with the C14 atom of FD44, (*ii*) Y52 and F55 recognize and clamp the right benzene ring through π–π interactions, and (*iii*) L182 main-chain carbonyl oxygen

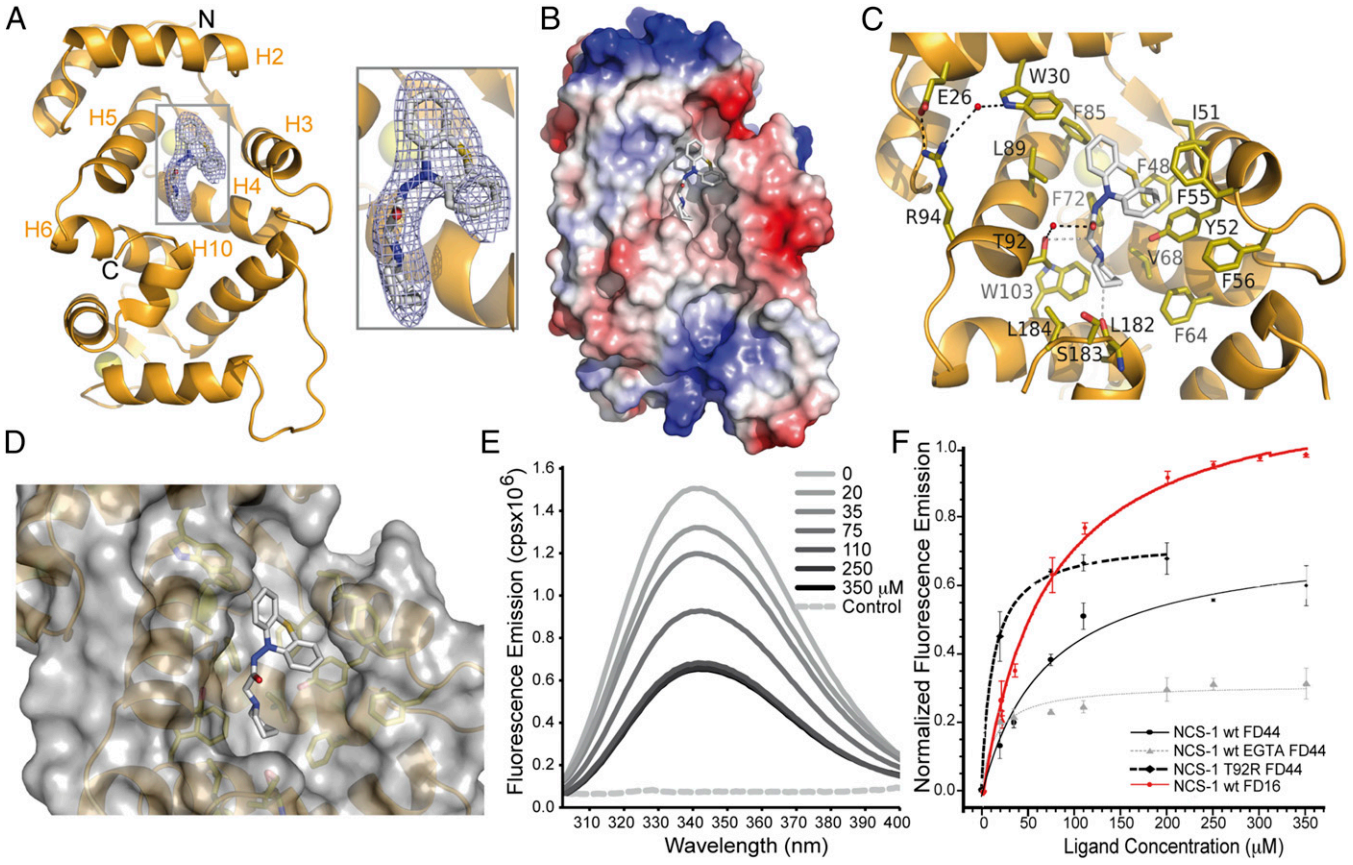

Fig. 3. Structure of the Ca^{2+}-loaded NCS-1 bound to aminophenothiazine FD44. (*A*) Ribbon representation of dNCS-1 in complex with Ca^{2+} (yellow spheres) and FD44 (stick mode; C, N, O, and S atoms shown in white, blue, red, and yellow, respectively). The $2F_o$-F_c electron density map for the small molecule is shown at 1.0σ. (*Inset*) A zoomed-in view of the gray-squared region. Helices contributing to FD44 pocket formation are indicated. (*B*) Electrostatic molecular surface of dNCS-1 showing the hydrophobicity of the FD44 cavity. (*C*) A detailed view of the residues interacting with FD44 compound. Strong and weak H bonds are shown with black and gray dashed lines, respectively. Water molecules are displayed as spheres. (*D*) Molecular surface representation on FD44 cavity as shown in *C*. (*E* and *F*) Fluorescence assays of FD44 and FD16 binding to NCS-1 in solution. (*E*) Trp fluorescence emission spectra of WT fly NCS-1 at increasing concentrations of FD44. Control: fluorescence of 350 μM FD44 in the absence of the protein. (*F*) Representation of the Trp fluorescence quenching of WT and T92R fly NCS-1 proteins with the ligand concentration (FD44 or FD16) in the presence of Ca^{2+} or EGTA. Data ± SD. The curves represent the least squares fitting to the experimental data considering a 1:1 stoichiometry. To properly compare the different curves, intensities were normalized and represented as $(I_0 - I)/I_0$ (*SI Materials and Methods*).

recognizes the FD44 piperidine ring, showing a weak H bond (O. . .HC) with the C16 atom of FD44 (Fig. 3*C*).

The aminophenothiazine FD16 conserves the same binding mode as FD44 and inserts into the same cavity with a similar contact area [339 Å^2 (30)] (Figs. S1*C* and S2 *A* and *B*). However, the chlorine atom present in the phenothiazine scaffold (Fig. 1*C*) allows a deeper insertion of FD16 in the cavity. The phenothiazine moiety presents an almost planar conformation, with the chlorine atom pointing out of the cavity. Compared with FD44, there is a 2.5-fold reduction of contacts in FD16. The missing interactions are found in the phenothiazine moiety and the piperazine group, which is poorly recognized with respect to the piperidine in FD44. In fact, helix H10 contacts the piperidine group through L182, S183, and L184, whereas in the complex with FD16, only the contacts with L182 are conserved.

The electron density in the CPZ complex clearly showed a disordered model of CPZ over two positions (molecules A and B) with site occupation factor of 0.5 (Fig. S1*D*). These CPZ molecules are located in the same cavity as FD44 and FD16, and they display different conformations (Fig. S2 *C* and *D*). (*i*) The angles between planes of the two benzene rings in the phenothiazine of molecules A and B are 139° and 150°, respectively. (*ii*) The phenothiazine substituent, the aliphatic amine in this case, is twisted in molecule A, whereas it is stretched in molecule B. The contact areas for CPZ molecules A and B are 260 and 188 Å^2 (30), respectively. CPZ is only recognized through the aminophenothiazine group, and the substituent is exposed to the solvent and completely disordered as the electron density map indicates (Fig. S1*D*). The C-terminal end of helix H10 is also disordered because of the lack of contacts with CPZ. Compared with FD44, H10 interactions with L182 and L184 are lost, and only a weak H bond with S183 is observed.

To measure the affinity of FD44 and FD16 to NCS-1 in solution and test the function of the cavity found in the crystal structures, we conducted a fluorescence assay. Because NCS-1 contains two Tryptophan residues W30 and W103, both located in the FD44 interaction surface (Fig. 3*C*), we monitored their fluorescence emission intensity at increasing amounts of the compounds. As shown in Fig. 3 *E* and *F*, FD44 and FD16 binding quenches the Tryptophan fluorescence. We used this spectroscopic change to follow the binding of these small molecules to WT dNCS-1 and a point mutant. The data show that, under Ca^{2+}-saturated conditions, the apparent K_d for FD44 is 71 ± 4 μM (Fig. 3*F*). Also, we mutated T92 in NCS-1, which establishes H bonds with FD44. The T92R substitution increased the affinity for FD44 10 times (K_d of 6.6 ± 1.4 μM) (Fig. 3*F*). Thus, the fluorescence data further validate our crystal structure and show that T92 is involved in the recognition of FD44. We repeated the fluorescence assay in the presence of EGTA, and the apparent K_d for FD44 changed to 22.2 ± 0.4 μM (Fig. 3*F*). Finally, we also measured the affinity of dNCS-1 to FD16, which showed a similar value (K_d of 69.6 ± 1.4 μM) (Fig. 3*F*).

The superimposition of the complex structures presented in this work with the previously solved, ligand-free dNCS-1, the one in which helix H10 is inserted into the crevice (19) (Fig. 1*A*), reveals the conformational change that the protein must suffer to accommodate the small compounds. The main changes occur in helix H3, which opens up, and helix H10, which moves backward to permit aminophenothiazine positioning (Fig. 4*A*). To illustrate this conformational change in more detail, we compared the above-mentioned ligand-free dNCS-1 structure with the dNCS-1/FD44 complex. The most notable changes are (*i*) W30, with side chain that rotates 90° to close the lid and hydrophobically interact with FD44; (*ii*) residues I51 and L89 that move backward to impede clashes with the S atom and the amide N atom of FD44, respectively; (*iii*) residues S183 and L184 from helix H10 that recognize the amine ring; and (*iv*) Y52 and F55 that clamp the phenothiazine group (Fig. 4*B*). These conformational changes reshape the large and exposed surface of NCS-1 to permit FD44 recognition (Figs. 3*D* and 4*C*), and helix H10, which is mobile in the ligand-free state (Fig. 1*A*), is stabilized inside the crevice through interactions with FD44 to prevent Ric8a interaction. Among the three tested compounds, FD44 is the one that contacts more extensively with helix H10. In fact, the ability of FD44 to inhibit the NCS-1/Ric8a complex is significantly reduced if helix H10 is deleted (Fig. S2 *E* and *F*).

Comparison of the *Drosophila* and human NCS-1 (23) structures suggests that the interaction with the human variant likely occurs as shown above, because the protein folding and all of the amino acids implicated in FD44 recognition are conserved (Figs. 1*B* and 4 *D* and *E*). As explained before, the main difference between the NCS-1 structures of the two species is found in helix H10 (Fig. 4*D*). In the human case, H10 is outside the crevice because of the presence of two pentaethyleneglycol molecules inside this cleft (23). However, as shown in *Drosophila* (19), this helix is also able to insert into the crevice (24).

NCS-1 and the Role of Myristoylation. NCS-1 is a myristoylated protein (31). There are a significant number of experimental observations that suggest that the human variant does not contain a Ca^{2+}/myristoyl switch mechanism. (*i*) The human protein is permanently bound to the cell membrane in the presence and absence of Ca^{2+} in vitro (31) and in vivo (32) and recently, also with synthetic membranes (33). (*ii*) O'Callaghan and Burgoyne (34) showed that hydrogen bonding between residues located in helix H1 (Fig. S3*A*) stabilizes the helix in a rigid conformation that could keep the N terminus of hNCS-1 in an open conformation with the myristoyl group exposed to the solvent, regardless the Ca^{2+} content. Interestingly, this hydrogen bonding is conserved in dNCS-1 (Fig. S3*B*), but it is not observed in the Ca^{2+} myristoyl switch NCS proteins (Fig. S3*A*). (*iii*) We had reported previously that the binding of *Drosophila* or human NCS-1 to Ric8a still occurs in the absence of Ca^{2+} (19). Those experiments were carried out in HEK cells, where proteins are myristoylated. Because we had also proved that the complete crevice in NCS-1 is the binding interface for Ric8a and that Ca^{2+} myristoyl switches use the myristoyl group to occlude the crevice in the absence of Ca^{2+}, our data do not favor a switch for NCS-1. (*iv*) Finally and related to the influence of myristoylation on FD44 binding, the crystal structure of NCS-1 bound to FD44 reveals many hydrophobic contacts with residues located in the N-terminal part of the crevice. Some proteins of the NCS family containing a Ca^{2+}/myristoyl switch use some of these amino acids to contact the myristoyl group (Fig. S3*A*). In this case, myristoylation could have an influence in FD44 binding.

To investigate this possibility, we performed coimmunoprecipitation (co-IP) assays in HEK cells, where NCS-1 undergoes myristoylation, and found that FD44 inhibits Ric8a binding at 20 μM (Fig. 2*B*). In solution and with the recombinant unmyristoylated protein, affinity for FD44 is 22 μM. These results suggest that myristoylation does not influence FD44 affinity. To test further the influence of myristoylation, we have found that a mutated form of NCS-1 that cannot be myristoylated binds Ric8a with the same affinity as the myristoylated version (Fig. S4). Also, FD44 shows interference of the NCS-1/Ric8 binding, irrespective of the myristoylation state of NCS-1 (Fig. S4). In conclusion, myristoylation does seem to have an effect on Ric8a binding or FD44 affinity, and these data, together with those previously reported, point to the absence of a Ca^{2+}/myristoyl switch in the fly and human NCS-1.

The Aminophenothiazine FD44 Modifies the Number of Synapses in a Genetic Model of Fragile X and Improves Learning Ability. Because FD44 and FD16 prevent the NCS-1/Ric8a interaction (Figs. 1*D* and 2) and we had previously identified the antagonistic effects of these two proteins on synapse number (19, 35), we assayed whether the two drug candidates could reduce synapse number in a pathological condition in which synapses are in excess (10). Fragile X is a convenient case for this assay, because the synaptic phenotype is well-characterized and the genetic origin is conserved (1). Mutants

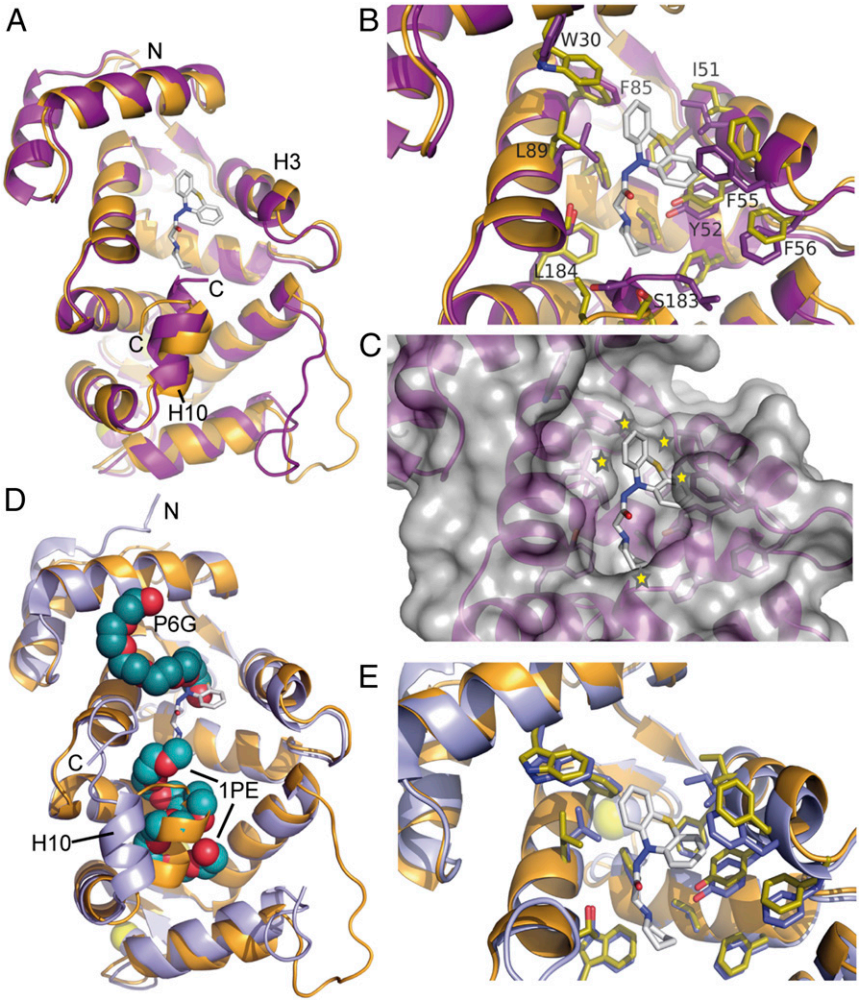

Fig. 4. Structural comparison of FD44-bound NCS-1 with related proteins. (*A*) Superimposition of the ligand-bound (orange ribbons) and helix H10-inserted ligand-free (purple ribbons; PDB ID code 4BY5) dNCS-1 structures. (*B*) A detailed view of the conformational change shown in *A*. All residues interacting with FD44 are shown, but only those showing a significant structural reorganization are labeled. (*C*) Molecular surface representation of the ligand-free dNCS-1. The ligand-bound structure was superimposed like in *A*, but only the FD44 molecule is depicted to show that the cavity of the apoprotein is too small to accommodate this compound, which would heavily clash (yellow stars) with the surrounding residues. It is interesting to compare this figure with Fig. 3*D* to clearly see the reshaping of the cavity on ligand binding. (*D* and *E*) Structural comparison of the dNCS-1/FD44 complex (orange ribbons) and the previously solved hNCS-1 structure (lilac ribbons; PDB ID code 1G8I). FD44 is shown in stick mode. PEG molecules (1× P6G and 2× 1PE) from the human crystal structure are shown in ball mode. (*E*) The view shows that residues implicated in FD44 recognition are conserved.

in *fmr1* show essentially the same synaptic phenotype in humans, mice, and flies (5, 11–13). Importantly, the fly homolog of NCS-1, Frq2, is among the mRNAs deficiently translated in *fmr1* mutants (20). We capitalized on these circumstances and the available structural and synaptic data about NCS-1 and Ric8a to directly test the potential effects of FD44 and FD16 on synapse number. To validate the specific tools for the planned experiments, we showed by Western blot that the mutant $fmr1^{\Delta 50}$ is null for protein expression (Fig. S5*A*), and we showed by RT-PCR assays that the $fmr1^{RNAi}$ effectively interferes with *fmr1* transcription (Fig. S5*B*).

$fmr1^{\Delta 50}$ Mutant larvae and the corresponding genetic controls were fed with FD44, FD16, or the solvent, DMSO, throughout larval development (*Materials and Methods* and Fig. 5). Synapse number and neuron volume were determined in an identified larval motor neuron at the late third instar (Fig. 5 *A* and *B*). The data confirmed that neuron volume is increased in the mutant (13, 36). Furthermore, we provide direct counting of synapses, which are also increased in the mutant (Fig. 5*A*). Notably, the pathological phenotype is largely suppressed by feeding FD44 to these larvae (Fig. 5 *A* and *B*). By contrast, FD44 or its solvent DMSO shows little or no effect on the controls. The result on the suppression of the aberrant number of synapses is fully consistent with the proposed function of the NCS-1/Ric8a interaction to control synapse number (19). The other drug candidate, FD16, proved less effective to reduce the aberrant number of synapses of the null *fmr1* mutant (Fig. 5 *A* and *B*).

Beyond the chronic effect of FD44 during development, we questioned if the drug could also have an acute effect. In addition, we questioned if the drug could ameliorate learning performance, a prominent feature of FXS syndrome. To these ends, we used the negatively reinforced associative olfactory learning paradigm in adult flies, in which FMRP levels had been abrogated because of the panneuronal expression of an interfering RNA-encoding transgene (Vienna *Drosophila* Resource Center; stockcenter.vdrc.at/control/main) and to which we administered the drug acutely. The use of an RNAi rather than a mutant allele in these experiments is justified because of the relatively low viability of adult mutant homozygotes. Also, driving the $fmr1^{RNAi}$ to the CNS allows for assaying the specific contribution of this tissue to learning. The data from $fmr1^{RNAi}$-expressing adults fed with the solvent DMSO show a strong learning deficit that phenocopies the effects of FMRP loss and are consistent with the larval synapse phenotypes (14, 37) (Fig. 5*E*). Remarkably, the learning deficit was ameliorated by 12 h of treatment with FD44 before training (Fig. 5*E*). As in larvae, feeding DMSO or FD44 to adult controls had little or no effect on learning, and the statistical analysis of the data does not reveal a significant difference in the learning index of control flies fed with FD44 vs. DMSO (Fig. 5*E*). These results are congruent with those on FD44-mediated suppression of aberrant synapse number in mutant larvae and provide a readily measurable acute behavioral effect of the drug in fully differentiated adult fly CNS neurons. Finally, learning indexes in the $fmr1^{RNAi}$-expressing animals were not modified by FD16 treatment (Fig. 5*F*). These results confirm the specificity of FD44 vs. other related molecules.

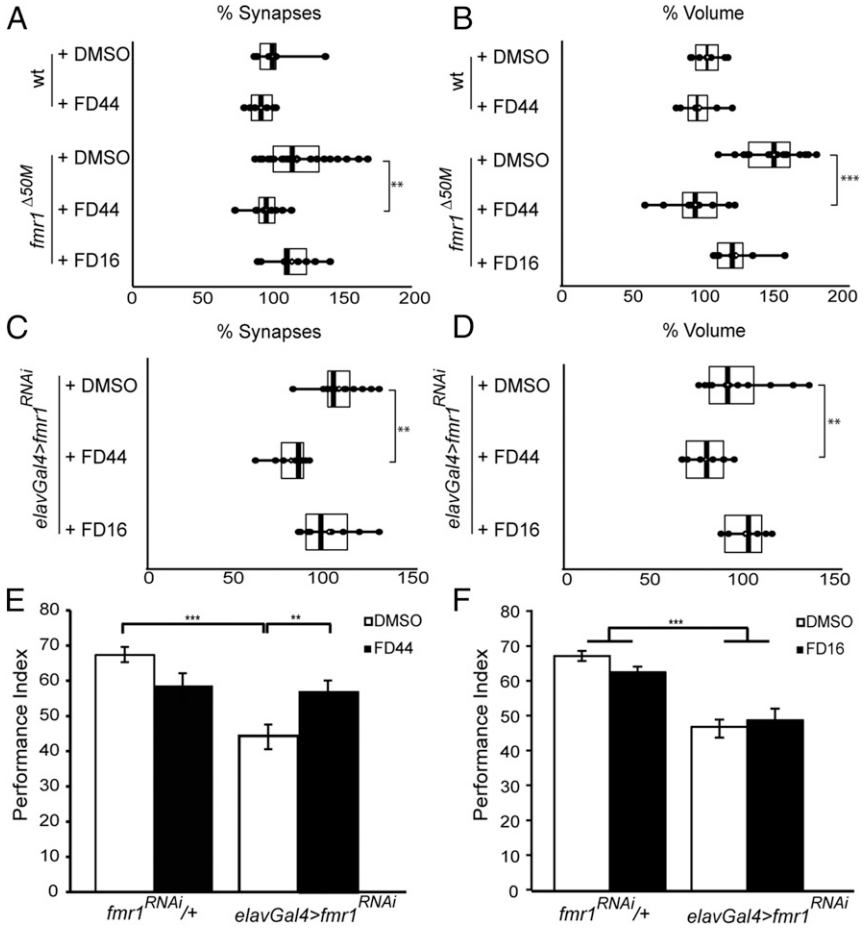

Fig. 5. Effects of FD44 and FD16 in vivo. (*A–D*) *Drosophila* WT or *fmr1* mutants were fed with 200 μM FD44, FD16, or DMSO, and larva III NMJs were analyzed. (*A*) Synapse number (nc82-positive spots) and (*B*) synapse volume from 7 to 15 NMJs of different larva were determined using Imaris over the confocal images. Similar measurements were performed on animals with panneuronally abrogated *fmr1* via RNAi, in which (*C*) synapse number and (*D*) volume were determined. Data are plotted in whisker graphs, where each dot represents one value, boxes represent interquartile ranges, vertical lines are the medians, and white diamonds are the averages. Data are shown as percentages of the control WT larva fed with DMSO. (*E* and *F*) *Drosophila* olfactory associative learning assay. Olfactory learning in a negatively conditioned paradigm was performed with control flies (fmr1 RNAi/+) or animals with panneuronally abrogated *fmr1* (*elavGal4* > $fmr1^{RNAi}$) after feeding them with 250 μM FD44, 250 μM FD16, or DMSO for 12 h before the assay. The performance index is shown. (*E*) $fmr1^{RNAi}$-expressing flies present the anticipated learning deficits, and their performance is significantly improved when fed with FD44 for 12 h, showing a learning index indistinguishable from that of control flies. (*F*) In contrast to the results with FD44 treatment, $fmr1^{RNAi}$-expressing flies present no amelioration in their learning performance when fed with FD16. FD16, like FD44, does not improve the learning performance of control flies. Data ± SD from 8 to 19 replicates, with 100 flies per experiment. Student's *t* test. $^{**}P = 0.01$; $^{***}P = 0.001$.

Discussion

By combining structural and chemoinformatic methodologies, we have discovered a small molecule, the phenothiazine derivative FD44, as a PPI inhibitor.

FD44 is biologically active and can prevent the aberrant increase of synapse number and the learning disability of a *Drosophila fmr1* fragile X model. The structural study has revealed the mechanism of action of FD44 in its interaction with NCS-1 for NCS-1/Ric8a complex inhibition. We had previously shown that helix H10 is mobile and functions as a built-in competitive inhibitor. Specifically, this helix is extruded out of the crevice for proper Ric8a recognition (19). In this context, FD44 is able to trap NCS-1 in an inactive conformation. The substituent attached to the phenothiazine group interacts with the C-terminal helix H10 and stabilizes it inside the crevice blocking the contact surface with Ric8a (Fig. 3*C*). Therefore, FD44 prevents the conformational change that helix H10 has to suffer to accept Ric8a. The fact that FD16 does not block helix H10 as efficiently as FD44 explains why this other derivative is not biologically effective. This study shows a potential therapeutic use of an aminophenothiazine and shows the versatility of these compounds. The substituents in the phenothiazine group promote specificity and drive these molecules to their corresponding targets, thus determining their biological activity (28). In fact, it has been also shown that another derivative, Trifluoperazine, can target the cancer-related Ca^{2+} binding protein S100A4, representing a potential inhibitor of metastasis (38).

In addition to the X-ray crystallography data, using a fluorescence assay, we show that FD44 interacts with NCS-1 in solution (Fig. 3 *E* and *F*). Under Ca^{2+}-saturating conditions, NCS-1 affinity for FD44 is 71 μM. However, affinity increases up to 22 μM in the presence of EGTA. This increment is relevant, because as we showed previously, the NCS-1/Ric8a complex is more stable in the absence of Ca^{2+} (19). Thus, the conditions in which FD44 displays its inhibitory properties are exactly the same as those of its efficient interaction with NCS-1. In agreement with all of these results, cell-based dose–response studies show that the formation of the NCS-1/Ric8a complex is prevented at 20 μM FD44 (Fig. 2 *A* and *B*).

The in vivo experiments show that feeding FD44 is an effective method to suppress the excess of synapse in the *Drosophila* FXS

model (Fig. 5 *A* and *C*). As previously reported, expression of NCS-1 is reduced and the number of synapses is increased in the fly *fmr1* mutant (13, 20). However, simultaneous overexpression of NCS-1 and Ric8a suppresses the synaptic phenotypes of each genetic alteration and yields a normal number of synapses (19). Here, the blockade of NCS-1/Ric8a interaction by FD44 should be equivalent to the simultaneous excess of free NCS-1 and Ric8a. Thus, the observed normal number of synapses in the FD44-treated *fmr1* mutant shows the consistency between the genetic and pharmacological experiments. Additional consistency is also found with FXS pathology data. cAMP levels are low in FXS, and antagonizing the cAMP-dependent phosphodiesterase PDE-4 rescues several phenotypes in the fly model (14, 39, 40). In this context, changes in cAMP are expected if the NCS-1/Ric8a binding is prevented, because the complex has an impact on Gs activity (19). Actually, the genetic increase of fly NCS-1 in the nervous system does produce a significant increase of cAMP levels as measured in head extracts (Fig. S6). Therefore, FD44 would be expected to increase the cAMP levels reduced in FXS, because abrogation of NCS-1/Ric8a binding should raise the free (uncomplexed) levels of both proteins. In any event, it must be pointed out that changes in cAMP represent a downstream effect from the molecular mechanism reported here.

Feeding FD44 to control flies did not affect viability or synapse number. In light of the available data, this innocuous effect is expected, because the number of synapses is determined by the balanced equilibrium between NCS-1 and Ric8a levels, and any treatments that maintain their ratio should lead to normalcy. Presumably, in the *fmr1* mutant, where NCS-1 levels are reduced, those of Ric8a would be relatively increased, and that condition leads to an increased number of synapses in accord with our prior report (19).

Aberrant synapse number and morphology have been shown to occur concurrently with learning and memory deficits (41, 42), but they were not directly linked to the behavior of the animals until now. FD44 restored the number of synapses in *fmr1* mutants (Fig. 5 *A* and *C*) and ameliorated the learning performance of adult flies (Fig. 5*E*), linking the number of synapses to the behavioral output of the mutant flies. Feeding control flies with FD44 or FD16 results in trends toward lower learning performance, but in all cases, they were not statistically different from controls (Fig. 5 *E* and *F*). It is also appropriate to point out that the parameter under evaluation is the learning index with variability that is well-known and documented. The effect of FD44 in adult flies under acute administration is relevant, because FXS diagnosis is typically achieved after the third year of life, although the synaptic aberration originates from embryonic stages.

Selectivity is an important issue in drug discovery. The 16 NCS family members show up to 60% sequence identity, all have similar topologies, and conserved hydrophobic residues within their crevice that participate in the recognition of their corresponding target also contact the myristoyl group or FD44 (Fig. 6 and Fig. S3*A*). However, each protein generates a unique 3D fold and exhibits important structural features in their hydrophobic crevice that determine target specificity and function (43, 44) and equally, will influence FD44 selectivity.

(*i*) The shape and size of the crevice, which are mainly determined by the ability of the protein to bind two or three Ca^{2+} ions, the positioning of the C-terminal helix H10, and the presence of a Ca^{2+}/myristoyl switch (43). The structure of the Recoverin/Rhodopsin kinase (RK25) (45) suggests that the aminophenothiazine ring of FD44 would not fit into the Recoverin crevice, because the different orientation of helix H5 generates a rather narrow crevice (Figs. 3 and 6). Regarding helix H10, it is important to note that it is one of the least conserved regions in sequence and length (Fig. S3*A*). It can be inside the crevice and contribute to target recognition, like in Recoverin or KChIP1 complexes (45, 46), or it can be out, like in dNCS-1/Ric8a (19) or Frq1/Pik1 (47, 48) complexes, where the targets fully occupy the crevice (Fig. 6). The dNCS-1/FD44 complex structure illustrates how important helix H10 is to shape the FD44 cavity. Thus, the different orientation, conformation, and dynamics of helix H10 will determine FD44 selectivity (Fig. 6).

(*ii*) Another important selectivity determinant is the presence of residues at the edge of the crevice that interact with the targets through strong polar contacts. For example, in the dNCS-1 isoforms, Frq1 and Frq2, an arginine at the edge of Frq2 crevice but not of Frq1 determines that Ric8a binds exclusively to Frq2 (19). These strong polar contacts are also found in other NCS/target complexes (Fig. 6) and the recognition of FD44 by T92 (Fig. 3*C*).

(*iii*) To understand selectivity, it will also be important to consider the affinities of the NCS proteins toward their targets. The reported affinities in Recoverin and ScFrq1 complexes shown in Fig. 6 are 1.4 and 0.1 μM, respectively. The moderate affinity of FD44 to NCS-1, which is in the 20-μM range, suggests that deleterious side effects are unlikely with these NCS proteins.

(*iv*) NCS-1 not only interacts with Ric8a (44). Although there is scarce information on the molecular mechanism of recognition and the relevance of the hydrophobic crevice for most of its targets (44), each interaction will have its unique structural requirement that would ensure selectivity. The structure solution of NCS-1 bound to Ric8a and other targets together with affinity calculations will be important to fully understand the mechanism of Ric8a inhibition by FD44 and rationalize, if necessary, the generation of FD44 derivatives with enhanced pharmacological properties toward the NCS-1/Ric8a or another NCS/target complex implicated in pathological processes.

Finally, small molecules are convenient for pharmacological therapy because of their ability to cross the blood–brain barrier and their easy administration. Although structurally related to CPZ, the derivative FD44 has revealed here unsuspected functions. The demonstration of its mechanism of action on the NCS-1/Ric8a interaction and the amelioration of synaptic and learning traits in FXS open a strategy to develop additional compounds that target this PPI for an eventual use in therapies against several forms of synaptopathies.

Materials and Methods

Additional methods, including the fly strains used, the behavioral studies, the crystallization and structure solution of the different dNCS-1/aminophenothiazine complexes, and the fluorescence experiments, are provided in *SI Materials and Methods*.

vs.

Ligand library preparation. The molecules from our in-house chemical library were prepared in Schrödinger Ligprep Wizard (Schrödinger Software Modules). The ligands were subjected to additional predocking preparations, where hydrogens were added followed by minimization and optimization with OPLS_2005 force field. Finally, 10 conformations for each ligand were generated and ready for docking.

VS using GLIDE. After preparing the ligand library and the protein, the grid was defined centering on R94. The library of small compounds was subjected to glide docking using the standard precision module.

Postdocking analysis. The molecules were ranked based on the scoring function GlideScore (GScore) (Table S1). GScore is an empirical scoring function that approximates the ligand binding free energy. It has many terms, including force field (electrostatic and van der Waals) contributions and terms rewarding or penalizing interactions known to influence ligand binding. It has been optimized for docking accuracy, database enrichment, and binding affinity prediction. To analyze the interactions of docked protein–ligand complexes, the Liginteractions module implemented in Maestro (Maestro Version 9.4.047; Schrödinger Software Modules) was used to check interactions between receptor and ligand atoms within a range of 4 Å.

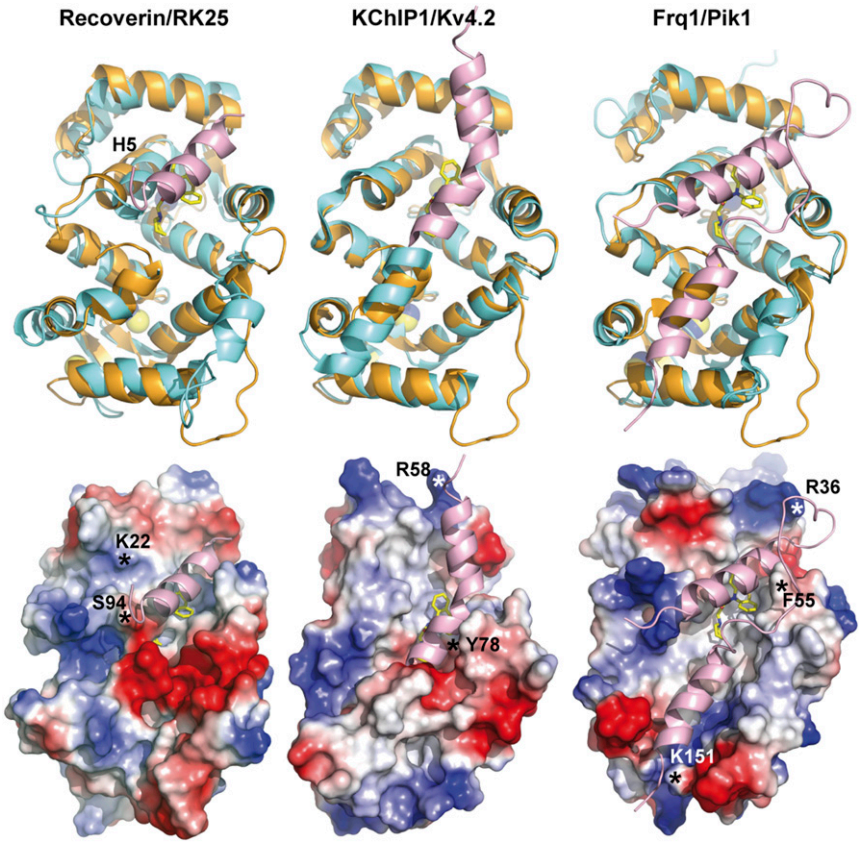

Fig. 6. Structural comparison of NCSs in complex with their targets. (*Upper*) Structure and (*Lower*) electrostatic molecular surface of Recoverin/RK25 [657-Å^2 contact area; PDB ID code 2I94 (45)], KChIP1/Kv4.2 [854-Å^2 contact area; PDB ID code 1S6C (46)], and Frq1/Pik1 [1,296-A^2 contact area; PDB ID code 2JU0 (47)] complexes. The structure of dNCS-1 (orange ribbons and yellow spheres representing Ca^{2+}) bound to FD44 (yellow sticks) was superimposed. NCSs and targets are shown as cyan and pink ribbons, respectively, and Ca^{2+} are shown as blue spheres. Asterisks indicate edge residues in NCSs interacting with their corresponding targets through H bonds or salt bridges (Fig. S3*A*). The comparison with NCS-1/FD44 complex (Fig. 3*B*) shows how different the hydrophobic grooves, their surroundings, and the orientation and fold of helix H10 are. Recoverin helix H5 is indicated to show its different orientation and consequences on crevice narrowness. In the KChIP1/Kv4.2 complex, helix H10 would clash with FD44, whereas in the Recoverin/RK25 complex, it would not reach the FD44 binding region.

Co-IP Assays and Western Blotting. The human NCS-1 construct (provided by R. D. Burgoyne, University of Liverpool, Liverpool, United Kingdom) was subcloned in pCDNA3.1, whereas the human Ric8a (a gift from G. Tall, University of Rochester Medical Center, Rochester, NY) was subcloned in nV5pCDNA3.1. *Drosophila* Ric8a, dNCS-1, and dNCS-1$^{\Delta H10}$ cloning and subcloning were previously described (19). The N-terminal G2A point mutation was performed with the Change-IT Directed Mutagenesis Kit (Affymetrix USB) following the manufacturer's instructions. These constructs were cotransfected into HEK293 cells using Lipofectamin (Invitrogen). DMSO-diluted compounds at the indicated concentrations or DMSO as control were added at the culture cells 24 h after transfection; 48 h after transfection, cells were lysated (buffer = 150 mM sodium chloride, 1.0% Nonidet P-40, 50 mM Tris, pH 8.0), and the compounds were added at the indicated concentrations in the lysis buffer and maintained throughout the immunoprecipitation assay. Precleared lysates were incubated overnight (12 h) at 4 °C with mouse anti–NCS-1 (1:500; Cell Signaling) or mouse anti-V5 (Invitrogen) as indicated in each experiment. Samples were subsequently incubated overnight with Protein-G–Sepharose (Sigma-Aldrich). After washing, proteins were eluted from the Sepharose and analyzed by Western blot following standard procedures; 10% of the lysate before immunoprecipitation was run as input. Mouse anti-V5 (1:2,000; Invitrogen) and rabbit anti–NCS-1 (1:1,000; Cell Signaling) or mouse anti–c-Myc (1:2,000; Sigma-Aldrich) antibodies were used for Western blot, and blots were incubated with mouse or rabbit TrueBlot (Rockland) as secondary antibodies to avoid heavy-/light-chain antibody interference.

***Drosophila* Synapse Counting Studies.** FD44 and FD16 were dissolved in DMSO and added to the fly culture media before solidification to ensure a homogeneous distribution in the vial at the final concentration of 200 μM. Eggs were laid down in these media, and larvae were raised at 25 °C until late LIII stage, when they were processed for synapse counting and volume analysis.

We used the glutamatergic neuromuscular junction (NMJ) of the female third larval instar as the experimental system. Synapses were visualized under confocal microscopy by the mAb nc82 (DSHB Hybridoma Bank), which identifies the Bruch pilot protein, a constituent of the presynaptic active zone (49), located at the edge of the characteristic T-bar specialization of fly synapses (50). Also, presynaptic nc82 spots correlate with postsynaptic GluRII clusters (49, 51). Throughout the text, we refer to nc82-positive spots as mature synapses. The axon profile was revealed by rabbit anti-HRP antibody (Jackson ImmunoResearch). All counts were obtained from muscle fiber 6/7 of the abdominal segment 3. Serial 1-μm confocal images were acquired in a Leica TSC SP5 Confocal Microscope and quantified by Imaris software. Experimental and control genotypes were run in parallel, and quantifications were done blindly.

ACKNOWLEDGMENTS. M.J.S.-B. thanks Alba Synchrotron (Xaloc Beamline) for access and support of the staff and Dr. Douglas Vinson Laurents (Institute "Rocasolano") for help with the fluorescence assay. This work was funded by the Spanish Ministry of Economy and Competitiveness (MINECO) with Grants BIO2011-28184-C02-02 and BFU2014-59796-R (to M.J.S.-B.) and BFU2012-38191 (to A.F.), European Cooperation in Science and Technology (COST) action "Proteostasis" (A.F. and E.M.C.S.), and "R&D" Pilot Project (M.J.S.-B.) from Instruct, part of the European Strategy Forum on Research Infrastructures. O.S. was supported by the Research Funding Program Thales—Investing in Knowledge Society through European Social Fund 376898. M.J.S.-B. is supported by a Ramón y Cajal Contract RYC-2008-03449 from MINECO.

1. Bagni C, Tassone F, Neri G, Hagerman R (2012) Fragile X syndrome: Causes, diagnosis, mechanisms, and therapeutics. *J Clin Invest* 122(12):4314–4322.
2. Busquets-Garcia A, Maldonado R, Ozaita A (2014) New insights into the molecular pathophysiology of fragile X syndrome and therapeutic perspectives from the animal model. *Int J Biochem Cell Biol* 53:121–126.
3. Wang H, Pati S, Pozzo-Miller L, Doering LC (2015) Targeted pharmacological treatment of autism spectrum disorders: Fragile X and Rett syndromes. *Front Cell Neurosci* 9:55.
4. Sastre A, Campillo NE, Gil C, Martinez A (2015) Therapeutic approaches for the future treatment of Fragile X. *Curr Opin Behav Sci* 4:6–12.
5. Darnell JC, et al. (2011) FMRP stalls ribosomal translocation on mRNAs linked to synaptic function and autism. *Cell* 146(2):247–261.
6. Tabet R, et al. (2016) Fragile X Mental Retardation Protein (FMRP) controls diacylglycerol kinase activity in neurons. *Proc Natl Acad Sci USA* 113(26):E3619–E3628.
7. Irwin SA, et al. (2001) Abnormal dendritic spine characteristics in the temporal and visual cortices of patients with fragile-X syndrome: A quantitative examination. *Am J Med Genet* 98(2):161–167.
8. Antar LN, Li C, Zhang H, Carroll RC, Bassell GJ (2006) Local functions for FMRP in axon growth cone motility and activity-dependent regulation of filopodia and spine synapses. *Mol Cell Neurosci* 32(1-2):37–48.
9. Grossman AW, Aldridge GM, Weiler IJ, Greenough WT (2006) Local protein synthesis and spine morphogenesis: Fragile X syndrome and beyond. *J Neurosci* 26(27):7151–7155.
10. Pfeiffer BE, Huber KM (2007) Fragile X mental retardation protein induces synapse loss through acute postsynaptic translational regulation. *J Neurosci* 27(12):3120–3130.
11. Hutsler JJ, Zhang H (2010) Increased dendritic spine densities on cortical projection neurons in autism spectrum disorders. *Brain Res* 1309:83–94.
12. Zhang YQ, et al. (2001) Drosophila fragile X-related gene regulates the MAP1B homolog Futsch to control synaptic structure and function. *Cell* 107(5):591–603.
13. Gatto CL, Broadie K (2008) Temporal requirements of the fragile X mental retardation protein in the regulation of synaptic structure. *Development* 135(15): 2637–2648.
14. Kanellopoulos AK, Semelidou O, Kotini AG, Anezaki M, Skoulakis EM (2012) Learning and memory deficits consequent to reduction of the fragile X mental retardation protein result from metabotropic glutamate receptor-mediated inhibition of cAMP signaling in Drosophila. *J Neurosci* 32(38):13111–13124.
15. Bolduc FV, Bell K, Cox H, Broadie KS, Tully T (2008) Excess protein synthesis in Drosophila fragile X mutants impairs long-term memory. *Nat Neurosci* 11(10):1143–1145.
16. Scotto-Lomassese S, et al. (2011) Fragile X mental retardation protein regulates new neuron differentiation in the adult olfactory bulb. *J Neurosci* 31(6):2205–2215.
17. Sun MK, Hongpaisan J, Alkon DL (2016) Rescue of synaptic phenotypes and spatial memory in young fragile X mice. *J Pharmacol Exp Ther* 357(2):300–310.
18. Dason JS, et al. (2009) Frequenin/NCS-1 and the Ca2+-channel alpha1-subunit coregulate synaptic transmission and nerve-terminal growth. *J Cell Sci* 122(Pt 22): 4109–4121.
19. Romero-Pozuelo J, et al. (2014) The guanine-exchange factor Ric8a binds to the Ca^{2+} sensor NCS-1 to regulate synapse number and neurotransmitter release. *J Cell Sci* 127(Pt 19):4246–4259.
20. Tessier CR, Broadie K (2011) The fragile X mental retardation protein developmentally regulates the strength and fidelity of calcium signaling in Drosophila mushroom body neurons. *Neurobiol Dis* 41(1):147–159.
21. Laraia L, McKenzie G, Spring DR, Venkitaraman AR, Huggins DJ (2015) Overcoming chemical, biological, and computational challenges in the development of inhibitors targeting protein-protein interactions. *Chem Biol* 22(6):689–703.
22. Guo W, Wisniewski JA, Ji H (2014) Hot spot-based design of small-molecule inhibitors for protein-protein interactions. *Bioorg Med Chem Lett* 24(11):2546–2554.
23. Bourne Y, Dannenberg J, Pollmann V, Marchot P, Pongs O (2001) Immunocytochemical localization and crystal structure of human frequenin (neuronal calcium sensor 1). *J Biol Chem* 276(15):11949–11955.
24. Heidarsson PO, et al. (2012) The C-terminal tail of human neuronal calcium sensor 1 regulates the conformational stability of the Ca^{2+}–activated state. *J Mol Biol* 417(1-2):51–64.
25. Ames JB, et al. (2000) Structure and calcium-binding properties of Frq1, a novel calcium sensor in the yeast Saccharomyces cerevisiae. *Biochemistry* 39(40):12149–12161.
26. González-Muñoz GC, et al. (2010) Old phenothiazine and dibenzothiadiazepine derivatives for tomorrow's neuroprotective therapies against neurodegenerative diseases. *Eur J Med Chem* 45(12):6152–6158.
27. González-Muñoz GC, et al. (2011) N-acylaminophenothiazines: Neuroprotective agents displaying multifunctional activities for a potential treatment of Alzheimer's disease. *Eur J Med Chem* 46(6):2224–2235.
28. López-Muñoz F, et al. (2005) History of the discovery and clinical introduction of chlorpromazine. *Ann Clin Psychiatry* 17(3):113–135.
29. Gifford JL, Walsh MP, Vogel HJ (2007) Structures and metal-ion-binding properties of the Ca2+-binding helix-loop-helix EF-hand motifs. *Biochem J* 405(2):199–221.
30. Krissinel E, Henrick K (2007) Inference of macromolecular assemblies from crystalline state. *J Mol Biol* 372(3):774–797.
31. McFerran BW, Weiss JL, Burgoyne RD (1999) Neuronal Ca(2+) sensor 1. Characterization of the myristoylated protein, its cellular effects in permeabilized adrenal chromaffin cells, Ca(2+)-independent membrane association, and interaction with binding proteins, suggesting a role in rapid Ca(2+) signal transduction. *J Biol Chem* 274(42):30258–30265.
32. O'Callaghan DW, et al. (2002) Differential use of myristoyl groups on neuronal calcium sensor proteins as a determinant of spatio-temporal aspects of Ca2+ signal transduction. *J Biol Chem* 277(16):14227–14237.
33. Lemire S, Jeromin A, Boisselier É (2016) Membrane binding of Neuronal Calcium Sensor-1 (NCS1). *Colloids Surf B Biointerfaces* 139:138–147.
34. O'Callaghan DW, Burgoyne RD (2004) Identification of residues that determine the absence of a Ca(2+)/myristoyl switch in neuronal calcium sensor-1. *J Biol Chem* 279(14):14347–14354.
35. Romero-Pozuelo J, Dason JS, Atwood HL, Ferrús A (2007) Chronic and acute alterations in the functional levels of Frequenins 1 and 2 reveal their roles in synaptic transmission and axon terminal morphology. *Eur J Neurosci* 26(9):2428–2443.
36. Morales J, et al. (2002) Drosophila fragile X protein, DFXR, regulates neuronal morphology and function in the brain. *Neuron* 34(6):961–972.
37. McBride SM, et al. (2005) Pharmacological rescue of synaptic plasticity, courtship behavior, and mushroom body defects in a Drosophila model of fragile X syndrome. *Neuron* 45(5):753–764.
38. Malashkevich VN, et al. (2010) Phenothiazines inhibit S100A4 function by inducing protein oligomerization. *Proc Natl Acad Sci USA* 107(19):8605–8610.
39. Kelley DJ, et al. (2008) The cyclic AMP phenotype of fragile X and autism. *Neurosci Biobehav Rev* 32(8):1533–1543.
40. Choi CH, et al. (2015) PDE-4 inhibition rescues aberrant synaptic plasticity in Drosophila and mouse models of fragile X syndrome. *J Neurosci* 35(1):396–408.
41. Sun MK, Hongpaisan J, Lim CS, Alkon DL (2014) Bryostatin-1 restores hippocampal synapses and spatial learning and memory in adult fragile x mice. *J Pharmacol Exp Ther* 349(3):393–401.
42. Volders K, et al. (2012) Drosophila rugose is a functional homolog of mammalian Neurobeachin and affects synaptic architecture, brain morphology, and associative learning. *J Neurosci* 32(43):15193–15204.
43. Ames JB, Lim S (2012) Molecular structure and target recognition of neuronal calcium sensor proteins. *Biochim Biophys Acta* 1820(8):1205–1213.
44. Burgoyne RD, Haynes LP (2015) Sense and specificity in neuronal calcium signalling. *Biochim Biophys Acta* 1853(9):1921–1932.
45. Ames JB, Levay K, Wingard JN, Lusin JD, Slepak VZ (2006) Structural basis for calcium-induced inhibition of rhodopsin kinase by recoverin. *J Biol Chem* 281(48):37237–37245.
46. Zhou W, Qian Y, Kunjilwar K, Pfaffinger PJ, Choe S (2004) Structural insights into the functional interaction of KChIP1 with Shal-type K(+) channels. *Neuron* 41(4):573–586.
47. Strahl T, et al. (2007) Structural insights into activation of phosphatidylinositol 4-kinase (Pik1) by yeast frequenin (Frq1). *J Biol Chem* 282(42):30949–30959.
48. Lim S, Strahl T, Thorner J, Ames JB (2011) Structure of a Ca2+-myristoyl switch protein that controls activation of a phosphatidylinositol 4-kinase in fission yeast. *J Biol Chem* 286(14):12565–12577.
49. Wagh DA, et al. (2006) Bruchpilot, a protein with homology to ELKS/CAST, is required for structural integrity and function of synaptic active zones in Drosophila. *Neuron* 49(6):833–844.
50. Hamanaka Y, Meinertzhagen IA (2010) Immunocytochemical localization of synaptic proteins to photoreceptor synapses of Drosophila melanogaster. *J Comp Neurol* 518(7):1133–1155.
51. Jordán-Álvarez S, Fouquet W, Sigrist SJ, Acebes A (2012) Presynaptic PI3K activity triggers the formation of glutamate receptors at neuromuscular terminals of Drosophila. *J Cell Sci* 125(Pt 15):3621–3629.
52. Acevedo SF, Froudarakis EI, Tsiorva AA, Skoulakis EM (2007) Distinct neuronal circuits mediate experience-dependent, non-associative osmotactic responses in Drosophila. *Mol Cell Neurosci* 34(3):378–389.
53. Tully T, Quinn WG (1985) Classical conditioning and retention in normal and mutant Drosophila melanogaster. *J Comp Physiol A Neuroethol Sens Neural Behav Physiol* 157(2):263–277.
54. Moressis A, Friedrich AR, Pavlopoulos E, Davis RL, Skoulakis EM (2009) A dual role for the adaptor protein DRK in Drosophila olfactory learning and memory. *J Neurosci* 29(8):2611–2625.
55. Pavlopoulos E, Anezaki M, Skoulakis EM (2008) Neuralized is expressed in the alpha/beta lobes of adult Drosophila mushroom bodies and facilitates olfactory long-term memory formation. *Proc Natl Acad Sci USA* 105(38):14674–14679.
56. Baños-Mateos S, Chaves-Sanjuán A, Mansilla A, Ferrús A, Sánchez-Barrena MJ (2014) Frq2 from Drosophila melanogaster: Cloning, expression, purification, crystallization and preliminary X-ray analysis. *Acta Crystallogr F Struct Biol Commun* 70(Pt 4): 530–534.
57. Kabsch W (2010) Xds. *Acta Crystallogr D Biol Crystallogr* 66(Pt 2):125–132.
58. Winn MD, et al. (2011) Overview of the CCP4 suite and current developments. *Acta Crystallogr D Biol Crystallogr* 67(Pt 4):235–242.
59. Adams PD, et al. (2010) PHENIX: A comprehensive Python-based system for macromolecular structure solution. *Acta Crystallogr D Biol Crystallogr* 66(Pt 2):213–221.
60. Allen FH (2002) The Cambridge Structural Database: A quarter of a million crystal structures and rising. *Acta Crystallogr B* 58(Pt 3 Pt 1):380–388.
61. Chen VB, et al. (2010) MolProbity: All-atom structure validation for macromolecular crystallography. *Acta Crystallogr D Biol Crystallogr* 66(Pt 1):12–21.
62. Schrödinger LLC (2013) The PyMOL Molecular Graphics System, Version 1.8.
63. Butterfield SM, Waters ML (2003) A designed beta-hairpin peptide for molecular recognition of ATP in water. *J Am Chem Soc* 125(32):9580–9581.
64. Ames JB, et al. (1997) Molecular mechanics of calcium-myristoyl switches. *Nature* 389(6647):198–202.
65. Stephen R, Bereta G, Golczak M, Palczewski K, Sousa MC (2007) Stabilizing function for myristoyl group revealed by the crystal structure of a neuronal calcium sensor, guanylate cyclase-activating protein 1. *Structure* 15(11):1392–1402.
66. Li C, Lim S, Braunewell KH, Ames JB (2016) Structure and calcium binding properties of a neuronal calcium-myristoyl switch protein, Vinisin-like protein 3. *PLoS One* 11(11):e0165921.